COMSOL
CONFERENCE
2024 FLORENCE

# A Comprehensive COMSOL Modeling for the Solar-Driven $CO_2$ Electroreduction to CO

M. Agliuzza[1], C.F. Pirri[1,2], A. Sacco[2]
1. Applied Science and Technology Department, Polytechnic University of Turin, Turin, Italy
2. Center for Sustainable Future Technologies @Polito, Italian Institute of Technology, Turin, Italy

## Abstract
Climate change is a short-term problem which can no longer be ignored and affects everything, from global food security to geopolitics and economics: extreme weather phenomena, falling crops yields, decrease of water availability, sea level rise, extinction of several animal species, are some of the many catastrophic consequences related to global warming. Carbon dioxide (CO2) is the primary greenhouse gas which contributes to climate change, due to its high residence time and radiative forcing. CO2 emission is primarily associated with the combustion of fossil fuels (which fulfills the 80% of the worldwide energy demand), heat generation and electricity. Growing demand in energy market speeds up the global energy consumption, leading to an increasing trend of CO2 concentration in air. In this framework, electrochemistry is the most promising process for decarbonization, since it allows the conversion of CO2 into added-value products in an up-scalable and sustainable technology. In this work, COMSOL® Multiphysics 6.1 software has been exploited to produce a comprehensive model for the electrochemical cell and validated through experimental results with good agreement. A 2D model is developed consisting of cathode and anode domains separated by an ion exchange membrane: Tertiary Current Distribution (TCD) has been employed for the cathodic and anodic compartments for the electrochemical and equilibrium reactions inside the electrolyte, and it has been coupled with a Secondary Current Distribution (SCD) physics for the ion exchange membrane domain. The catalysts for Oxygen Evolution Reaction and CO2 reduction reaction (Platinum foil and silver nanoparticles, respectively) are modeled by infinitely thin films at the boundaries of the domain, by feeding the Butler-Volmer equations with their electrochemical parameters in the TCD physics. The model successfully replicates the experimental data for the conversion of CO2 into Carbon Monoxide (CO) and can predict the performance of the device by varying different parameters (e.g., voltage applied, inflow electrolyte velocity, dimension of the cell). Moreover, chemical conditions at the electrode surfaces can be inspected, such as variation of chemical species concentrations and pH in the diffusive boundary layers. In addition, the integration with photovoltaics as electrical source is implemented as well: the model simulates the electrochemical cell integrated with a Dye-Sensitized Solar Cells, such that the performance of the device as a function of the solar irradiance can be predicted. Modeling the electrochemical setup is a powerful tool not only to predict and optimize the operational conditions of the device, but also to follow the scaling-up process of the technology and its integration into more complex systems.
**Keywords:** $CO_2$ conversion, electrochemistry, model, PV-EC, carbon monoxide

## Introduction
The Carbon Dioxide ($CO_2$) electrochemical reduction is a promising approach for both mitigating $CO_2$ emissions and producing renewable fuels or chemicals. In particular, it is a process that uses electricity to convert $CO_2$ into value-added chemicals or fuels, such as carbon monoxide (CO), formic acid (HCOOH), methane ($CH_4$) and $C_{2+}$ products [1]. This technology has gained attention for its mild conditions, in terms of pressure and temperature requirements, non-toxic green electrolytes and repeatability of the results. The key components of the design include the electrocatalysts, which are the active materials that facilitate the $CO_2$ Reduction Reaction ($CO_2$RR) by lowering its energy barrier [2], the electrolyte and the energy power source. In fact, it is often emphasized that a renewable energy source (*e.g.* solar energy) is wanted to promote a carbon-neutral and sustainable process. In this framework, a lot of efforts have been made in literature to optimize experimentally the coupling between the Photovoltaics module and the electrochemical cell for $CO_2$ reduction (PV-EC) [3-6], along with the modeling for the $CO_2$RR reactor [7-11]: in this work it is presented a mathematical model for the solar-driven $CO_2$RR implemented in COMSOL® Multiphysics, in which the energy harvesting system is treated through its governing equation: the simulations are validated through experimental results, to guarantee the reliability of the results.

## Experimental Set Up
The device studied and modeled in this present work is a PV-EC system (*Artificial Leaf*), in which the energy harvesting system is a module of 6 Dye-Sensitized Solar Cells integrated in series, and the $CO_2$RR reactor is a batch electrochemical cell with recirculation of the electrolyte. The main challenge

for such PV-EC devices consists in the operational electric point of the system: in absence of an external current source, in fact, the system finds its natural working point (in terms of Current and Voltage) in the superimposition between the I-V characteristics of the PV and EC modules. Since the solar-to-fuel efficiency heavily depends on this, the operational point must lay in a region where the selectivity toward the specific product is the highest, and the solar cell works near its maximum power point. For these reasons, it is important to study and optimize the two devices separately, before the integration. In the following, the two systems are described thoroughly, and some experimental characterizations are given.

**Batch Cell Reactor**

In a standard batch cell configuration, the electroreduction of $CO_2$ occurs solely at the cathode's interface, thanks to a metallic catalyst which lowers the potential barrier and favors the reaction. In the case of CO production, the electrochemical reactions occurring are the $CO_2$RR (reaction (1)) and Hydrogen Evolution Reaction (HER, reaction (2)) at the cathode, while Oxygen Evolution Reaction (OER, reaction (3)) occurs at the anode interface:

$$CO_2 + 2H^+ + 2e^- \leftrightarrow CO + H_2O \quad (1)$$
$$2H^+ + 2e^- \leftrightarrow H_2 \quad (2)$$
$$2H_2O \leftrightarrow 4H^+ + 4e^- + O_2 \quad (3)$$

The electrochemical reactor is a batch cell, which comprises an anodic and cathodic compartment separated by an ion-exchange membrane (Fig. 1). The electrolyte used is an aqueous 0.1 M $KHCO_3$ recirculated through external reservoirs thanks to two peristaltic pumps; the electrolyte is saturated with $CO_2$, which is directly injected into the reactor at a volumetric mass flow of 15 ml $min^{-1}$. At the cathode, Ag nanoparticles are deposited through sputtering technique on a Carbon Paper substrate (with a current of deposition of 50 mA and time of 300 seconds) for the CO production, while commercial Pt foil is exploited at the anode for an efficient and non-limiting OER.

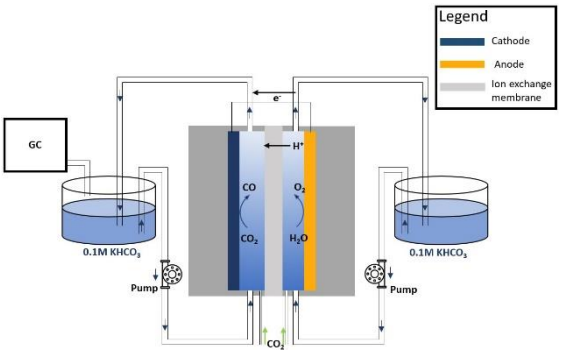


*Figure 1. Diagram of the experimental setup. Reprinted with permissions under the terms of the CCA 4.0. [7]*

In an engineering approach, the main figure of merits of the setup are the Faradaic Efficiency (Fig.2) and Current Density (Fig.3) curves, which describe the selectivity toward the specific product and the rate of production, respectively. By looking at the FE curves in Fig.2, the results confirm the theory for which the trend is not monotonic, but it rather exhibits a potential window in which $CO_2$RR is favored with respect to HER. At low voltages, in fact, the potential is not sufficient to satisfy the overpotential required for triggering the $CO_2$ reduction, while at high potentials (V > 4V) the rate-limiting step is related to the high consumption of $CO_2$ at the electrode's interface, along with a

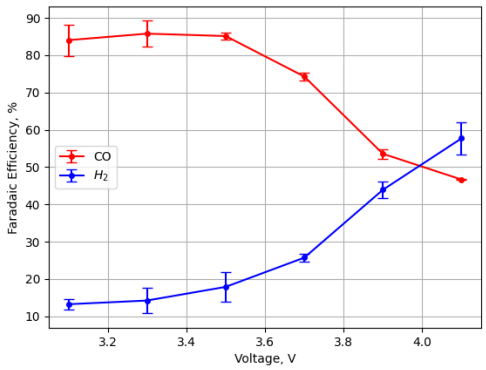


*Figure 2. Faradaic Efficiencies of CO and $H_2$. The x-axis refers to the voltage applied in a 2-electrode configuration.*

insufficient mass transfer of $CO_2$ molecules from the bulk toward the cathode. In these results, it is not depicted the trend at low potential, since the products in that are region are so small that the Gas Chromatography cannot detect them. As it will be shown later, the simulations will confirm the hypothesis. Please note that all the results reported are in a 2-electrode configuration and the experiments are performed by chrono-amperometries for 1 hour.

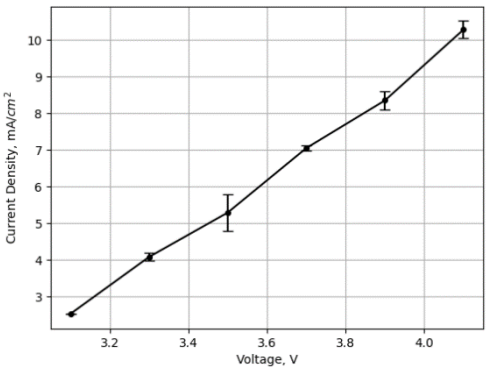


*Figure 3 Current density as a function of the Voltage applied.*

**Photovoltaics Module**

The solar cell is a diode in which a Photocurrent $I_{ph}$ can be produced by photogeneration of carriers (electron, holes): the $I_{ph}$ shifts the Current-Voltage characteristics of the diode in dark conditions, such that a positive power can be extracted, and energy is generated. Depending on the generation of the photovoltaics, the carriers are photogenerated through different physical phenomena: in the present work, third generation Dye-Sensitized Solar cells (DSSCs) are exploited. In contrast with the typical cells based on semiconductive materials, DSSCs are photoelectrochemical devices in which charge transport and charge photogeneration are separate mechanisms [12]: electrons are photogenerated in a light-sensitive Ruthenium-based dye, and are collected by $TiO_2$ nanoparticles deposited on a conductive FTO glass. The electrons are then regenerated by an Iodide/Triiodide redox couple in the electrolyte at the Pt counter electrode. Since the single DSSC is not enough to power the electrochemical cell, a module consisting of 6 DSSCs and joined by conductive Ag paste. In Fig.4, it is reported the IV characteristics of the module as a function of the irradiance, expressed in Suns (where 1 sun = 1 kW/m$^2$).

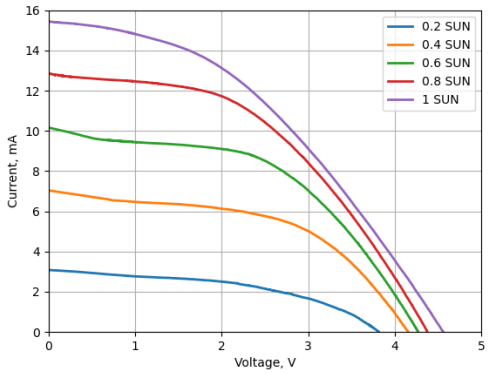


*Figure 4. IV curves of the photovoltaic module, as a function of the irradiance.*

## Numerical Model

The governing equations for the PV-EC device are implemented in a 2D model on COMSOL® Multiphysics 6.1, exploiting the Electrochemistry Module. The Batch cell Model here reported has already been published, for more information the reader is invited to consult the Ref. [7].

**EC Model**

The backbone of the reactor model is a 2D geometry (Fig.5), comprising of three main domains: cathodic/anodic compartments and the membrane domain. A $CO_2$-saturated 0.1M aqueous $KHCO_3$ electrolyte is modeled inside the compartments, with recirculation through inlet/outlet boundaries. Ag nanoparticles and Pt foil are modeled as infinitely thin films at the boundaries of the simulation domain, where the main electrochemical reactions occur.

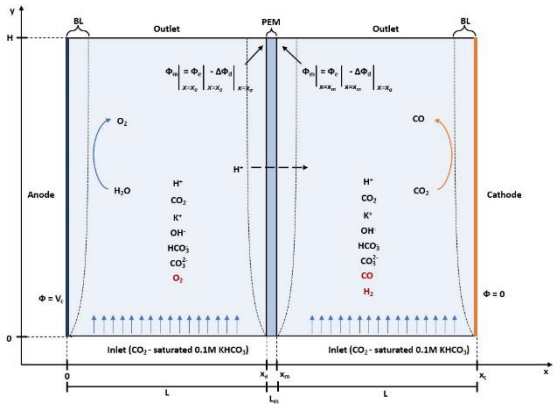


*Figure 5. Schematic representation of the simulation domain. L represent the cell semi-length, and $\Phi_m$, $\Phi_e$ and $\Phi_d$ are the membrane/electrolyte and Donnan potential respectively. Reprinted with permissions under the terms of the CCA 4.0. [7]*

**Electrolyte Domain** The electrolyte is modeled through Tertiary Current Distribution (TCD), by introducing the main chemical species (i.e. $CO_2$, $K^+$, $OH^-$, $HCO^-_3$, $CO_3^{2-}$, $H^+$, $H_2$, CO, $O_2$). When $CO_2$ dissolves in water, in fact, several chemical reactions occur so fast that they can be considered in equilibrium in all the domain, in particular carbonate/bicarbonate reactions and water self-ionization process:

$$H_2O \overset{K_f}{\Leftrightarrow} H^+ + OH^- \qquad K_f \qquad (4)$$

$$HCO_3^- + OH^- \overset{K_1}{\Leftrightarrow} CO_3^{2-} + H_2O \qquad K_1 \qquad (5)$$

$$CO_2 + OH^- \overset{K_2}{\Leftrightarrow} HCO_3^- \qquad K_2 \qquad (6)$$

with $K_f = 10^{-14}$ M$^2$, $K_1 = 4.66 \times 10^3$ 1/M and $K_2 = 4.44 \times 10^7$ M (from *Sullivan et al.* [13]).
The ionic current distribution $J_e$ is expressed as

$$J_e = F \sum_i z_i N_i \qquad (7)$$

where F is the Faraday constant, $z_i$ and $N_i$ the charge number and ionic mass flux of the i-th species (please note that only ions contribute to the current distribution).
The latter term may be calculated by means of the Nernst-Planck equations:

$$N_i = \underbrace{-D_i \nabla c_i}_{diffusion} - \underbrace{z_i u_{mob,i} F c_i \nabla \phi_e}_{migration} + \underbrace{c_i u}_{convection} \qquad (8)$$

Where in the first diffusion term, $D_i$ is the diffusion coefficient and $c_i$ the species concentration; in the second migration term, $u_{mob,i}$ refers to the species mobility, and $\phi_e$ the electrolyte potential; lastly, in the convection term, $u$ is the velocity. The mobility is calculated by means of the Nernst-Einstein relation:

$$u_{mob,i} = \frac{D_i}{RT} \quad (9)$$

where $R$ is the molar gas constant and $T$ the temperature. The electroneutrality condition in the electrolyte holds:

$$\sum_i z_i c_i = 0 \quad (10)$$

Regarding the species mass continuity, the following equation holds in the electrolyte domain:

$$\nabla \cdot \mathrm{N}_i + u \cdot \nabla \mathrm{c}_i = R_i \quad (11)$$

where $R_i$ is the mass source term for each species. $R_i$ is equal to 0 in the electrolyte (where only equilibrium reactions occur) and different from zero only on the cathode/anode boundaries, where consumption/formation of reactants/products happen. Finally, the charge conservation is considered:

$$\nabla \cdot \mathrm{J}_e = 0 \quad (12)$$

The chemical species initial concentrations and diffusion coefficients used are reported in [7].

**Membrane Domain** The Nafion 117 ion-exchange membrane is modelled through the Secondary Current Distribution (CD). Since no significant concentration gradients are expected, in this case the current distribution in the membrane $i_m$ is expressed by the Ohm's law

$$i_m = -\sigma_m \Delta\Phi_m \quad (12)$$

Since only $H^+$ can pass through, the molar flux of protons $N_{H^+}$ is calculated:

$$n \cdot N_{H^+} = \frac{n \cdot i_m}{F} \quad (13)$$

where n is the normal direction of the membrane interface.

At the membrane domain boundaries, the potential shift is given by the Donnan potential $\Phi_d$, which can predict the membrane potential

$$\Delta\Phi_d = \frac{RT}{F} \ln\left(\frac{[H^+]}{C_m}\right) \quad (14)$$

where $C_m$ is the fixed charge concentration (1M). The potential on the membrane $\Phi_m$, therefore, can be calculated considering the contribution of the Donnan potential on the membrane boundaries:

$$\Phi_m = \Phi_e - \Delta\Phi_d \quad (15)$$

**Cathode/Anode Boundaries** In the electrode boundaries, the electrochemical reactions (Eq. 1,2,3) occur. To determine the partial current densities $j_{par}$, which is to say the percentage of current density used for each electrochemical reaction, the Butler vomer equations are exploited in the Concentration-dependent form:

$$j_{par} = j_0 \left[C_R exp\left(\frac{\alpha_a F}{RT}\eta\right) - C_{OX} exp\left(-\frac{\alpha_c F}{RT}\eta\right)\right] \quad (16)$$

The equation relates the partial current density to the overpotential $\eta$ of the reaction, through two main kinetic parameters: anodic/cathodic charge transfer coefficients ($\alpha_a, \alpha_c$) and the exchange current density $j_0$. The parameter $C_R$ is set equal to 1, while $C_{OX}$ is equal to one for the $CO_2$RR, and for HER:

$$\mathrm{C}_o = \frac{C^s_{CO_2}}{C^*_{CO_2}} \quad (17)$$

In this way, it can be modeled the mass-transfer limit of the $CO_2$ molecules from the bulk ($C^*_{CO_2}$) to the surface ($C^s_{CO_2}$). The kinetic parameters used ($\alpha_a, \alpha_c$, $j_0$) are reported in the previous work [7].

The overpotential is expressed by the difference of the applied potential on the electrode ($\Phi_s$) and the equilibrium potential for the reaction to occur (r= $CO_2$RR, HER, OER):

$$\eta_r = \Phi_s - \mathrm{E}_{o,r} - \Phi_e \quad (18)$$

At last, a mass source term is introduced in the normal species flux on the electrodes surfaces due to the electrochemical reactions:

$$n \cdot N_i = \frac{\nu_i j_{par}}{nF} \quad (19)$$

where $\nu_i$ are the stoichiometric coefficients of the species involved in the reactions, and $n$ the number of electrons involved.

The FEs reported in the model results come from the following equation

$$\mathrm{FE}_{\square} = \frac{j_{par}}{J_{tot}} \times 100 \quad (20)$$

where $J_{tot}$ is the total current density.

**Numerical processing** Finite Element Method (FEM) is used to solve the PDEs through a user-defined rectangular mesh. The mesh contains 782 boundary elements and 19095 domain elements. Both stationary and time-dependent simulations are performed.

**PV Model**

The PV has been inserted in the model by exploiting the governing equation of the electrical equivalent circuit, called the one-diode model:

$$I = I_{ph} - I_0 \left[exp\left(\frac{V + IR_s}{nV_t}\right) - 1\right] - \frac{V + IR_s}{R_{sh}} \quad (21)$$

where $I_{ph}$ is the photogenerated current, $I_0$ the saturation current, $R_s$ the series resistance, n the ideality factor, $V_t$ the thermal voltage (approx. 25 mV at ambient T), $R_{sh}$ the Shunt Resistance. The equation is fitted through the experimental IV characteristics, and the parameters are retrieved: the equation is then used as electrical source in the COMSOL® model. In future refinements, a

relationship between the irradiance and the diode model will be found, to retrieve the energy production as a function of the illumination conditions.

## Results

Let us now investigate the main results retrieved by the experiments and the model

### EC Model Validation

At first, the model has been validated with experimental results, to check the reliability of the simulations. Fig.6 reports the FEs and Current Density curves as a function of the Voltage applied for two different lengths L of the reactor: in both cases, the model fits well the experimental data. The velocity of the electrolyte is set to u= 0.0057 m $s^{-1}$ and u=0.0067 m $s^{-1}$, which correspond to a volumetric mass flow of 15 ml $min^{-1}$ for the reactors with semi-cell length L = 0.6 cm (Fig. 6 a,c) and L = 0.25 (Fig. 6 b,d) respectively. The simulation also validates the hypothesis that, at low voltages, HER prevails with respect to CO production.

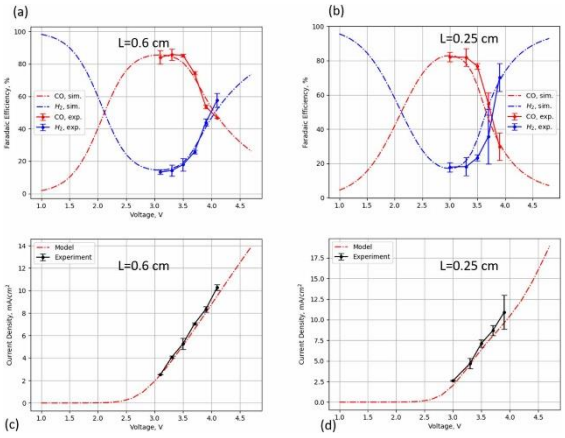


*Figure 6. Faradaic efficiency and Current density from simulation (dotted lines) and experimental results (straight lines) for two different dimensions of the reactor. Reprinted with permissions under the terms of the CCA 4.0. [7]*

### PV integration

In Fig. 7 it is depicted the superimposition between the experimental IV curves of the PV and EC modules, which leads to the operational point of the device: the system should work at a $V_{op}$= 3.1V and a $I_{op}$=8.6 mA, which corresponds to approximately 3.4 mA $cm^{-2}$. For model validation purposes, the diode model (Eq. 21) is now retrieved by fitting the experimental IV curves (Fig.4) and extrapolating the main electrical parameters (Fig. 8), such that it can be inserted into the COMSOL® simulations. It can be noticed that the shunt resistance $R_{sh}$ decreases with the incident power, with an increase of the photogenerated current; the series resistance, on the other hand, is almost constant.

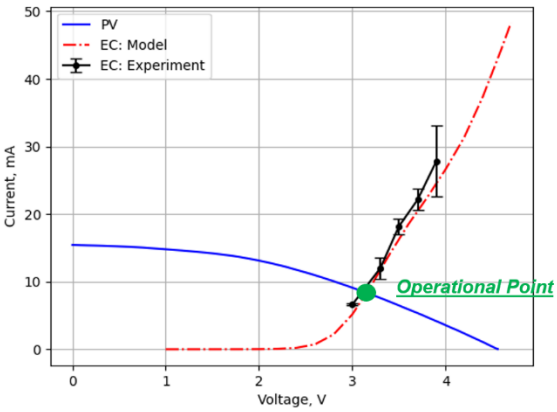


*Figure 7. Superimposition of the experimental IV characteristics of the PV (blue line) and EC (red dotted line model, black straight line experimental).*

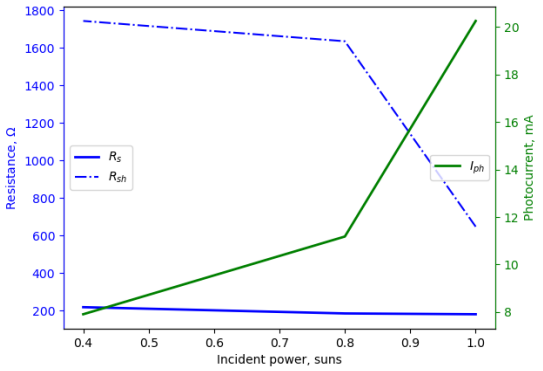


*Figure 8. Electrical parameters extrapolated from the fitting of the IV characteristics of the PV module.*

Lastly, the diode equation is used in the COMSOL® model to check the validity of the whole PV-EC simulation. For this purpose, a time-dependent simulation is performed, such that a chronoamperometric experiment can be reproduced. The result of the simulation output is depicted in Fig. 9. Not only the model validates the operational point of the devices, but it also interestingly shows the transient of the electrochemical reactor before it converges to the stationary values.

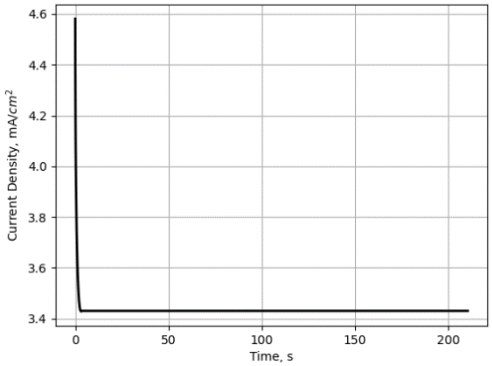


*Figure 9. Current density retrieved by the time-dependent study of the COMSOL® model.*

## Conclusions

A comprehensive COMSOL® 2D model of the PV-EC device is reported. The present model not only is able to predict the chemical conditions punctually in the domain and the performance of the device for the $CO_2$RR, but it paves the way for an all-around comprehensive model which integrates the PV technology as well. In future works, the system will be optimized to predict the performance as a function of the incident power, to check the CO production in low-light conditions (*e.g.* cloudy weather). Moreover, the time-dependent simulation will be further inspected, to retrieve useful information about the transient of the $CO_2$RR mechanism.

## References

[1] R. Lin, J. Guo, X. Li, P. Patel, and A. Seifitokaldani, "Electrochemical Reactors for CO2 Conversion," *Catalysts*, vol. 10, no. 5.

[2] B. Kumar *et al.*, "New trends in the development of heterogeneous catalysts for electrochemical CO2 reduction," *Catalysis Today*, vol. 270, pp. 19-30, 2016.

[3] M. Agliuzza, A. Mezza, and A. Sacco, "Solar-driven integrated carbon capture and utilization: Coupling CO2 electroreduction toward CO with capture or photovoltaic systems," *Applied Energy*, vol. 334, p. 120649, 2023.

[4] C. E. Creissen and M. Fontecave, "Solar-Driven Electrochemical CO2 Reduction with Heterogeneous Catalysts," *Advanced Energy Materials*, vol. 11, no. 43, p. 2002652, 2021.

[5] Gurudayal *et al.*, "Efficient solar-driven electrochemical CO2 reduction to hydrocarbons and oxygenates," *Energy & Environmental Science*, 10.1039/C7EE01764B vol. 10, no. 10, pp. 2222-2230, 2017.

[6] J. Kim, S. Jeong, M. Beak, J. Park, and K. Kwon, "Performance of photovoltaic-driven electrochemical cell systems for CO2 reduction," *Chemical Engineering Journal*, vol. 428, p. 130259, 2022.

[7] M. Agliuzza, C. F. Pirri, and A. Sacco, "A comprehensive modeling for the CO2 electroreduction to CO," *Journal of Physics: Energy*, vol. 6, no. 1, p. 015004, 2024.

[8] S. Chinnathambi, M. Ramdin, and T. J. H. Vlugt, "Mass Transport Limitations in Electrochemical Conversion of CO2 to Formic Acid at High Pressure," *Electrochem*, vol. 3, no. 3, pp. 549-569.

[9] N. Gupta, M. Gattrell, and B. MacDougall, "Calculation for the cathode surface concentrations in the electrochemical reduction of CO2 in KHCO3 solutions," *Journal of Applied Electrochemistry*, vol. 36, no. 2, pp. 161-172, 2006.

[10] Y. Kotb, S.-E. K. Fateen, J. Albo, and I. Ismail, "Modeling of a Microfluidic Electrochemical Cell for the Electro-Reduction of CO2 to CH3OH," *Journal of The Electrochemical Society*, vol. 164, no. 13, p. E391, 2017.

[11] K. Wu, E. Birgersson, B. Kim, P. J. A. Kenis, and I. A. Karimi, "Modeling and Experimental Validation of Electrochemical Reduction of CO2 to CO in a Microfluidic Cell," *Journal of The Electrochemical Society*, vol. 162, no. 1, p. F23, 2015.

[12] M. Grätzel, "Dye-sensitized solar cells," *Journal of Photochemistry and Photobiology C: Photochemistry Reviews*, vol. 4, no. 2, pp. 145-153, 2003.

[13] B. P. Sullivan, K. Krist, and H. E. Guard, "Electrochemical and electrocatalytic reactions of carbon dioxide," 1993.

## Acknowledgements

The author Matteo Agliuzza would like to thank the Italian Ministry of Education (MIUR) for the Ph.D. fellowship funded under the National Research and Innovation Operational Program 2014–2020 (CCI 2014IT16M2OP005), ESF REACT-EU resources, Action IV.4 'Doctorates and research contracts on innovation topics' and Action IV.5 'Doctorates on Green topics'. This study was also developed in the framework of the research activities carried out within the Project “Network 4 Energy Sustainable Transition—NEST”, Spoke ...: ....., Project code PE0000021, funded under the National Recovery and Resilience Plan (NRRP), Mission 4, Component 2, Investment 1.3— Call for tender No. 1561 of 11.10.2022 of Ministero dell’Universita` e della Ricerca (MUR); funded by the European Union—NextGenerationEU.